Inorganic Chemistry

pubs.acs.org/IC

Communication

Energy Landscape for the Electrocatalytic Oxidation of Water by a Single-Site Oxomanganese(V) Porphyrin

Dong Wang and John T. Groves*

Cite This: *Inorg. Chem.* 2022, 61, 13667−13672

Read Online

ACCESS | Metrics & More | Article Recommendations | Supporting Information

ABSTRACT: A cationic manganese porphyrin, Mn^{III}-TDMImP, is an efficient, homogeneous, single-site water oxidation electrocatalyst at neutral pH. The measured turnover frequency for oxygen production is 32 s^{-1}. Mechanistic analyses indicate that $Mn^{V}(O)(OH_2)$, the protonated form of the corresponding *trans*-$Mn^{V}(O)_2$ species, is generated from the $Mn^{III}(OH_2)_2$ precursor in a 2-e^- two-proton process and is responsible for O−O bond formation with a H_2O molecule. Chloride ion is a competitive substrate with H_2O for the $Mn^{V}(O)(OH_2)$ oxidant, forming hypochlorous acid with a rate constant that is 3 orders of magnitude larger than that of water oxidation. The data allow the construction of an experimental energy landscape for this water oxidation catalysis process.

The oxidation of water to molecular oxygen (O_2) in photosystem II (PS II) converts solar photons to an electrical potential that is subsequently utilized to reduce CO_2 to biomass. This energy-demanding reaction is catalyzed by the Mn_4Ca oxygen-evolving complex (OEC), which accumulates four oxidizing equivalents in each cycle before the key O−O bond formation and subsequent O_2 evolution occur.[1] Synthetic analogues of the OEC have provided a large inventory of metal-based water oxidation catalysts (WOCs).[2] Among these, manganese WOCs are mostly multinuclear;[3] single-site Mn catalysts are rare but have shown suggestive reactivity.[3b,4] Mechanistic and computational studies have shown that a high-valent Mn^{V}=O species is capable of making an O−O bond via intermolecular or intramolecular pathways,[4e,5] supporting the hypothesis that O−O bond formation at a single-site high-valent Mn center is feasible.[5c,6]

The water-soluble, cationic manganese porphyrin Mn^{III}-TDMImP [**1**; TDMImP = 5,10,15,20-tetrakis(1,3-dimethylimidazol-2-yl)porphyrin] is unusually well-behaved and has enabled a comprehensive understanding of this redox system. The steric hindrance of the dimethylimidizolium groups prevents dimerization, and the positive charges near the porphyrin *meso*-carbon atoms both increase the Mn oxidation potentials and lower the Mn−OH_2 pK_a values. A high-valent *trans*-dioxomanganese derivative, $Mn^{V}(O)_2$-TDMImP (**2**), is stable at alkaline pH, allowing its characterization by spectroscopic means.[7] Further, oxo transfer between **2** and halide ions (Cl and Br) was found to be fast and reversible.[8] At neutral and alkaline pH, these equilibria favor the formation of **2**. Direct measurement of these equilibrium constants revealed that the redox potential of the $Mn^{V}(O)_2/Mn^{III}(OH_2)_2$ couple is only 100−200 mV below that of H_2O_2/H_2O at acidic pH.[8] Furthermore, heterolytic O−O bond cleavage of a hydroperoxo species, HOO-Mn^{III}-TDMImP (**3**), to form **2** was found to have a very low activation enthalpy ($\Delta H^{\ddagger}$ = 4.2 kcal/mol).[9] Together, these results suggested that the reverse process, O−O bond formation, could also be facile (Scheme 1).

Scheme 1. Interconversion of 3 and oxoMn^{V}-TDMImP Complexes (2 and 4)

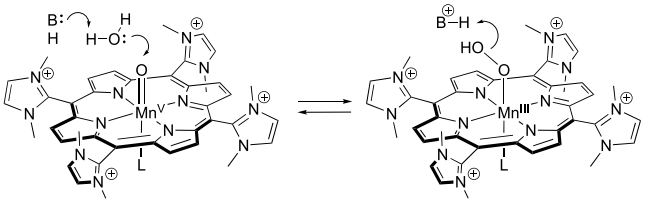

TDMImPMn^{V}=O **2**: L = O^{2-}
4: L = OH_2

TDMImPMn^{III}-O-OH **3**: L = OH_2

Here, we describe an electrochemical WOC process by this manganese porphyrin (**1**) at neutral pH. An unusually fast turnover frequency of 32 s^{-1} has been observed that involves $Mn^{V}(O)(OH_2)$ (**4**) and its conjugate base, $Mn^{V}(O)_2$ (**2**). Chloride ion is a competitive substrate with H_2O for the oxidant **4**, having a rate constant ~10^3-fold faster than that of water oxidation. These results have afforded an unusual opportunity to construct an energy landscape for this Mn-WOC.

A significant catalytic current developed at an onset potential of ~1100 mV versus Ag/AgCl (Figure 1A) during scanning of the cyclic voltammogram (CV) of 1 mM **1** in 0.1 M Na-Pi buffer at pH 7. A plot of the catalytic current measured at 1400 mV versus the concentration of **1** gave a

Received: June 30, 2022
Published: August 22, 2022

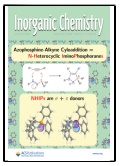

https://doi.org/10.1021/acs.inorgchem.2c02284
Inorg. Chem. 2022, 61, 13667−13672

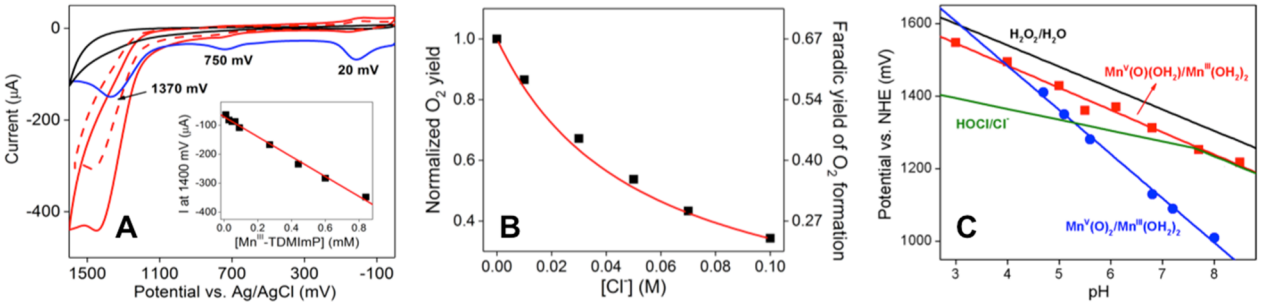

Figure 1. (A) CV curves for 1 mM **1** in 0.1 M Na-Pi at pH 7 in H_2O (red), D_2O (dashed red), and a buffer background (black). The SWV curve (blue) shows redox waves at 20, 750, and 1370 mV, assigned to Mn^{III}/Mn^{II}, Mn^{IV}/Mn^{III}, and Mn^{V}/Mn^{IV}, respectively. Inset: Plot of i_{cat} at 1400 mV versus [**1**] and the best linear fit (red). (B) Plot of the O_2 faradaic (right) and normalized (left) yields as a function of $[Cl^-]$ (best fit to eq 1, red). (C) Nernstian plots of the potential versus pH for the $Mn^{V}(O)(OH_2)/Mn^{III}(OH_2)_2$ (red) and $Mn^{V}(O)_2/Mn^{III}(OH_2)_2$ (blue) couples. The red and blue lines are the best linear fits. The H_2O_2/H_2O (black) and $HOCl/Cl^-$ (green) couples are shown for comparison.

linear correlation (Figure 1A, inset) similar to the Co analogue Co-TDMImP,[10] indicating that **1** is a single-site catalyst.[11] O_2 evolution was observed with **1** under the same electrolytic conditions with a faradaic yield of ∼70% using a Clark electrode (Figure S1). By contrast, electrolysis at pH 9 afforded the *trans*-dioxomanganese(V) complex **2** (Figure S2). A smaller catalytic current was observed when WOC was carried out in D_2O, indicating a solvent kinetic isotope effect of 3 (see Figure 1A and the Supporting Information, SI), typical of a concerted O-atom-proton transfer process.[2n,10,12] The normalized catalytic current decreased with increasing scan rate (ν) from 10 to 500 mV/s (Figure S3A), indicating that O−O bond formation is rate-determining.[13] A plot of i_{cat}/i_{diff} (catalytic current/diffusional current) for the $Mn^{III/II}$ couple at 20 mV) versus $1/\nu^{1/2}$ gave a linear correlation (Figure S3A), allowing a k_{obs,H_2O} value of 32 s^{-1} for the WOC to be calculated.[10] Foot-of-the-wave analysis afforded 42 s^{-1} (Figure S3B),[2n,14] comparable to an immobilized manganese porphyrin dimer described by Naruta et al.[3c] and ∼2 orders of magnitude faster than other Mn-based systems.[15] Only **1** was observed during electrocatalysis; negligible decomposition was observed over hours of turnover (Figure S4). A series of controls demonstrated that **1** is a homogeneous catalyst, not a precursor of any oxide species (Figures S5−S7).[16]

We then examined the effect of added chloride ions on the water oxidation activity. At pH 7, the thermodynamic 2-e^- oxidation potential of Cl^- is ∼90 mV (2 kcal/mol) lower than that of H_2O.[17] A significant increase of the catalytic current was observed upon the addition of Cl^- to **1** (Figures S8 and S9); added nitrate had no effect. Moreover, the faradaic yield of O_2 evolution exhibited a 3-fold nonlinear decrease upon the addition of Cl^- ion from 0 to 0.1 M (Figure 1B). Clearly, chloride ion is a competitive substrate with H_2O, intercepting the reactive Mn oxidant. In such a competition, the faradaic yield of O_2 evolution can be expressed as eq 1

$$O_2\% = \frac{2k_{obs,H_2O}}{2k_{obs,H_2O} + k_{obs,Cl^-}} = \left(1 + \frac{k_{2,Cl^-}}{2k_{2,H_2O}}\frac{[Cl^-]}{[H_2O]}\right)^{-1} \quad (1)$$

where k_{2,H_2O} and k_{2,Cl^-} are second-order rate constants for the oxidation of H_2O and Cl^-, respectively. The data shown in Figure 1B fit well to eq 1, with a value of $k_{2,Cl^-}/k_{2,H_2O}$ of 2.1 × 10^3, fitting the Swain−Scott nucleophilicity parameters for chloride-in-water reactions.[18] With k_{obs,H_2O} = 32 s^{-1} for water oxidation, k_{2,Cl^-} was determined to be 1.2 × 10^3 M^{-1} s^{-1} at pH 7. The ratio $k_{2,Cl^-}/k_{2,H_2O}$ thus corresponds to a difference of 4.5 kcal/mol in the activation free energy for these two reactions.

Below the WOC onset potential, CV and square-wave voltammogram (SWV) features were observed at 20 mV (ΔE = 70 mV) and 750 mV (Figure 1A), assigned to the $Mn^{III/II}$ and $Mn^{IV/III}$ couples, respectively.[8b] Importantly, an additional SWV wave at 1370 mV, assigned to Mn^{IV}/Mn^{V}, lies under the catalytic wave, indicating that this Mn^V species is the reactive WOC oxidant. SWV measurements of these three redox couples from pH 3.0 to 8.5 (Figure S10 and Table S1) provide several key mechanistic insights. The $Mn^{IV/III}$ potential shifts significantly with the pH, while those for $Mn^{V/IV}$ and $Mn^{III/II}$ were relatively unchanged. The measurement of these 1-e^- potentials thus allows us to calculate the 2-e^- $Mn^{V/III}$ potential (eq 2).

$$E(Mn^{V/III}) = \frac{E(Mn^{V/IV}) + E(Mn^{IV/III})}{2} \quad (2)$$

The plot of $E(Mn^{V/III})$ (red points) versus pH gave a linear correlation (Figure 1C). The slope of −61 mV/pH clearly indicates that the Mn^{III}/Mn^{V} oxidation is associated with the transfer of *two protons*. Catalyst **1** is a diaqua species, $Mn^{III}(OH_2)_2$ at pH 7, with previously determined pK_a values of 7.8 and 8.7.[7] Thus, the active species generated at the electrode surface is inferred to be an oxo−aqua complex (**4**) from this Nernstian plot slope. This species (**4**) has also been proposed as the active oxidant in the oxygenation of Br^- in our previous studies because of the obvious acid catalysis.[8a,19] The oxo−hydroxo complex $Mn^{V}(O)(OH)$ is not likely because it requires the transfer of 2e^- + 3H^+ from $Mn^{III}(OH_2)_2$ and the corresponding Nernstian plot slope would be −90 mV/pH. A stable dimeric bis[$Mn^{V}(O)(OH)$] porphyrin also required acid to produce O_2, further implicating **4**.[3c,5a]

We propose the mechanism depicted in Scheme 2 to explain this Mn-mediated WOC. Generation of the reactive oxo-Mn^V species **4** requires the transfer of two electrons and two protons from a $Mn^{III}(OH_2)_2$ resting state (Figure 1C). Nucleophilic attack of H_2O at the manganyl oxygen atom in **4** would then form an O−O bond and generate the well-characterized HOO-Mn^{III} species **3**, which undergoes further oxidation to produce O_2.[9] Meanwhile, the known reaction of $Mn^{V}(O)_2$ (**2**) with Cl^- as a competing substrate, forming hypochlorite,[8b] would divert Mn^V directly back to Mn^{III}, reducing the yield of O_2. A fraction of **4** diffusing from the

https://doi.org/10.1021/acs.inorgchem.2c02284
Inorg. Chem. 2022, 61, 13667−13672

Scheme 2. Proposed Mechanism for Water Oxidation Catalyzed by 1

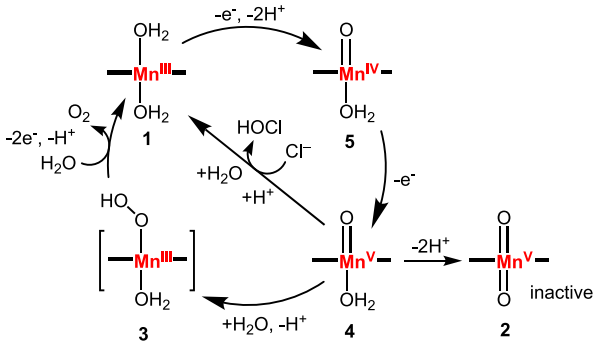

electrode surface forming **2**[9] would also lower the faradaic yield of O_2.

Oxo transfer between **2** and Cl^- or Br^- (eq 3) is fast and reversible, with measurable, pH-dependent equilibrium constants (Figure 1C, blue points).[8]

$$Mn^{V}(O)_2 + X^- + 4H^+ \rightleftarrows Mn^{III}(OH_2)_2 + XO^- \quad (3)$$

A slope of −121 mV/pH (blue line) indicates a $2e^- + 4H^+$ process, consistent with its assignment to the $Mn^{V}(O)_2/Mn^{III}(OH_2)_2$ couple. Figure 1C clearly shows that **4** is more oxidizing than **2** at neutral pH with a free energy difference of ∼180 mV (4.1 kcal/mol). Over the entire pH range studied, the potential of the $Mn^{V}(O)(OH_2)/Mn^{III}(OH_2)_2$ couple is ∼60 mV lower than that of the H_2O/H_2O_2 couple, corresponding to a $\Delta G°$ deficiency of only ∼1.4 kcal/mol for water oxidation. At neutral pH, the oxidation of Cl^- by **4** is thermodynamically favorable. By contrast, the $Mn^{V}(O)_2/Cl^-$ equilibrium greatly favors $Mn^{V}(O)_2$ (**2**) + Cl^-.[8b]

The Nernstian electrochemical behavior and turnover kinetics for WOC reported here, along with our previous results describing the O−O bond scission kinetics for Mn^{III}-OOH and equilibrium data for reversible chloride oxidation by this same manganese porphyrin, present an opportunity to construct an experimentally determined energy landscape for the key manganese species involved in this WOC and competitive inhibition by a chloride ion. The differences in ΔG (Scheme 3, red numbers) can be calculated from the Nernstian plots in Figure 1C. The activation energy for O−O bond heterolysis (14.7 kcal/mol) derives from the kinetics of the conversion of **3** to **2**.[9] Also the 4.5 kcal/mol difference in the activation energies for the oxidation of water and Cl^- to form **6** can be calculated from the ratio (2.1×10^3) of the rate constants for these two reactions determined in the present work. We assumed that the O−O bond cleavage and formation reactions proceed through a similar transition state. Both reactions involve the transfer of a single proton: a "push−pull" mechanism in the former case[9] and deprotonation of water in the latter case, which is the microscopic reverse.

The *trans*-dioxo-Mn^V porphyrin **2** is the most stable species at pH 7, while its oxo−aqua form **4** is 4.1 kcal/mol higher (Scheme 3). This prototropy is consistent with the experimental findings that reactions of **1** with chemical oxidants (H_2O_2 and ClO^-) above pH 7 yield **2**, not **4**, as the detectable product in solution, as we have reported.[7−9] The reverse processes, namely, the oxygenation of H_2O and Cl^- by **2** at pH 7, are both endergonic and kinetically disfavored according to the experimental data in Scheme 3. By contrast,

Scheme 3. Energy Landscape (kcal/mol) for the Interconversions of Mn-TDMImP Species Involved in H_2O and Cl^- Oxygenation Reactions at pH 7 with Experimentally Determined Thermodynamic (Red) and Kinetic (Blue) Values (See the SI for Derivations)

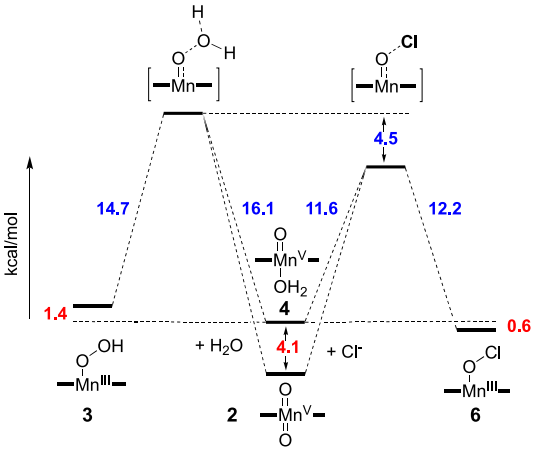

the reactive species **4** is nearly isoenergetic with Mn^{III}-OOH (**3**) and Mn^{III}-OCl, enabling O−O or O−Cl bond formation by **4**. Electrochemical oxidation is a unique way of generating **4** at the electrode surface. Significantly, the oxidation of H_2O by **4** is facile and only slightly endergonic. The activation barrier for O−O bond formation is 4.5 kcal/mol higher than that of the formation of an O−Cl bond, despite the fact that the difference in the driving force for the two reactions is only 2 kcal/mol. This difference probably reflects the higher intrinsic nucleophilicity of chloride over water.[18]

This Mn-WOC system is less reactive than the Co analogue,[10] which we attribute to the relative stabilities of **4** and an oxocobalt(IV) porphyrin cation radical. Very recently, an oxomanganese(V) corrole was found to mediate WOC in nonaqueous solutions.[5b] The aqueous system **1** shows a faster O−O bond formation rate (∼0.6 vs 0.0044 M^{-1} s^{-1}) and a lower activation free energy (16.1 vs 22.2 kcal/mol) compared to the manganese corrole system.

The observation that chloride interferes with O_2 formation is intriguing. The role of Cl^- near Mn4 in PS II is unclear. It has been proposed that Cl^- is involved in a hydrogen-bonding network that facilitates a proton-transport pathway near the OEC of the PS II.[20] While this loosely bound chloride seems to be located too far away to be directly associated with Mn4,[21] a functional role has been considered.[22] A role for the HOCl/Cl^- couple as a 2-e^- redox "buffer" could be suggested from the results presented here.

In summary, **1** catalyzes electrochemical water oxidation at neutral pH and is one of the most active single-site manganese water oxidation electrocatalysts reported to date. This Mn system is based on characterized intermediates, directly measured kinetics, and measured equilibrium constants. The results reveal that a transient species **4** generated at the electrode surface is responsible for O−O bond formation with water. A chloride ion was found to compete with water, reacting with **4** 10^3-fold faster than H_2O. The electrochemical, kinetic, and equilibrium data for the various Mn-TDMImP species allow the construction of an experimentally determined energy diagram for H_2O and Cl^- oxygenation that may afford a more quantitative understanding of these reactivities.

https://doi.org/10.1021/acs.inorgchem.2c02284
Inorg. Chem. 2022, 61, 13667−13672

■ ASSOCIATED CONTENT

Supporting Information

The Supporting Information is available free of charge at https://pubs.acs.org/doi/10.1021/acs.inorgchem.2c02284.

Additional experimental details, methods, and materials, Table S1, and Figures S1−S10 (PDF)

■ AUTHOR INFORMATION

Corresponding Author

John T. Groves − *Department of Chemistry, Princeton University, Princeton, New Jersey 08544, United States;* orcid.org/0000-0002-9944-5899; Email: jtgroves@princeton.edu

Author

Dong Wang − *Department of Chemistry, Princeton University, Princeton, New Jersey 08544, United States;* Present Address: Department of Chemistry and Biochemistry, University of Montana, Missoula, MT 59812

Complete contact information is available at: https://pubs.acs.org/10.1021/acs.inorgchem.2c02284

Notes

The authors declare no competing financial interest.

■ ACKNOWLEDGMENTS

Support of this research by the National Science Foundation (Grants CHE-1464578 and CHE-1900048) is gratefully acknowledged. Initial aspects were supported by the Center for Catalytic Hydrocarbon Functionalization, an Energy Frontier Research Center, U.S. Department of Energy, Office of Science, Basic Energy Sciences, under Award DE-SC0001298.

■ REFERENCES

(1) (a) Najafpour, M. M.; Renger, G.; Hołyńska, M.; Moghaddam, A. N.; Aro, E.-M.; Carpentier, R.; Nishihara, H.; Eaton-Rye, J. J.; Shen, J.-R.; Allakhverdiev, S. I. Manganese Compounds as Water-Oxidizing Catalysts: From the Natural Water-Oxidizing Complex to Nanosized Manganese Oxide Structures. *Chem. Rev.* **2016**, *116*, 2886−2936. (b) Yano, J.; Yachandra, V. Mn4Ca Cluster in Photosynthesis: Where and How Water is Oxidized to Dioxygen. *Chem. Rev.* **2014**, *114*, 4175−4205. (c) Yang, K. R.; Lakshmi, K. V.; Brudvig, G. W.; Batista, V. S. Is Deprotonation of the Oxygen-Evolving Complex of Photosystem II during the S-1 -> S-2 Transition Suppressed by Proton Quantum Delocalization? *J. Am. Chem. Soc.* **2021**, *143*, 8324−8332. (d) Cox, N.; Pantazis, D. A.; Lubitz, W. Current Understanding of the Mechanism of Water Oxidation in Photosystem II and Its Relation to XFEL Data. In *Annual Review of Biochemistry*; Kornberg, R. D., Ed.; Annual Reviews, 2020; Vol. *89*, pp 795−820. (e) Pantazis, D. A. Missing Pieces in the Puzzle of Biological Water Oxidation. *ACS Catal.* **2018**, *8*, 9477−9507. (f) Suga, M.; Akita, F.; Yamashita, K.; Nakajima, Y.; Ueno, G.; Li, H. J.; Yamane, T.; Hirata, K.; Umena, Y.; Yonekura, S.; Yu, L. J.; Murakami, H.; Nomura, T.; Kimura, T.; Kubo, M.; Baba, S.; Kumasaka, T.; Tono, K.; Yabashi, M.; Isobe, H.; Yamaguchi, K.; Yamamoto, M.; Ago, H.; Shen, J. R. An Oxyl/oxo Mechanism for Oxygen-oxygen Coupling in PSII Revealed by an X-ray Free-electron Laser. *Science* **2019**, *366*, 334−338. (g) Young, I. D.; Ibrahim, M.; Chatterjee, R.; Gul, S.; Fuller, F. D.; Koroidov, S.; Brewster, A. S.; Tran, R.; Alonso-Mori, R.; Kroll, T.; Michels-Clark, T.; Laksmono, H.; Sierra, R. G.; Stan, C. A.; Hussein, R.; Zhang, M.; Douthit, L.; Kubin, M.; de Lichtenberg, C.; Vo Pham, L.; Nilsson, H.; Cheah, M. H.; Shevela, D.; Saracini, C.; Bean, M. A.; Seuffert, I.; Sokaras, D.; Weng, T. C.; Pastor, E.; Weninger, C.; Fransson, T.; Lassalle, L.; Brauer, P.; Aller, P.; Docker, P. T.; Andi, B.; Orville, A. M.; Glownia, J. M.; Nelson, S.; Sikorski, M.; Zhu, D. L.; Hunter, M. S.; Lane, T. J.; Aquila, A.; Koglin, J. E.; Robinson, J.; Liang, M. N.; Boutet, S.; Lyubimov, A. Y.; Uervirojnangkoorn, M.; Moriarty, N. W.; Liebschner, D.; Afonine, P. V.; Waterman, D. G.; Evans, G.; Wernet, P.; Dobbek, H.; Weis, W. I.; Brunger, A. T.; Zwart, P. H.; Adams, P. D.; Zouni, A.; Messinger, J.; Bergmann, U.; Sauter, N. K.; Kern, J.; Yachandra, V. K.; Yano, J. Structure of Photosystem II and Substrate Binding at Room Temperature. *Nature* **2016**, *540*, 453−457.

(2) (a) Zhang, X. P.; Chandra, A.; Lee, Y. M.; Cao, R.; Ray, K.; Nam, W. Transition Metal-mediated O-O Bond Formation and Activation in Chemistry and Biology. *Chem. Soc. Rev.* **2021**, *50*, 4804−4811. (b) Sutradhar, M.; Pombeiro, A. J. L.; da Silva, J. A. L. Water Oxidation with Transition Metal Catalysts with Non-innocent Ligands and Its Mechanisms. *Coord. Chem. Rev.* **2021**, 439. (c) Nakazono, T.; Wada, T. Photochemical Water Oxidation Using a Doubly N-Confused Hexaphyrin Dinuclear Cobalt Complex. *Inorg. Chem.* **2021**, *60*, 1284−1288. (d) Liu, C.; Qian, J.; Ye, Y. F.; Zhou, H.; Sun, C. J.; Sheehan, C.; Zhang, Z. Y.; Wan, G.; Liu, Y. S.; Guo, J. H.; Li, S.; Shin, H.; Hwang, S.; Gunnoe, T. B.; Goddard, W. A.; Zhang, S. Oxygen Evolution Reaction Over Catalytic Single-site Co in a Well-defined Brookite TiO_2 Nanorod Surface. *Nat. Catal.* **2021**, *4*, 36−45. (e) Geer, A. M.; Musgrave, C.; Webber, C.; Nielsen, R. J.; McKeown, B. A.; Liu, C.; Schleker, P. P. M.; Jakes, P.; Jia, X. F.; Dickie, D. A.; Granwehr, J.; Zhang, S.; Machan, C. W.; Goddard, W. A.; Gunnoe, T. B. Electrocatalytic Water Oxidation by a Trinuclear Copper(II) Complex. *ACS Catal.* **2021**, *11*, 7223−7240. (f) Zhang, B. B.; Sun, L. C. Artificial Photosynthesis: Opportunities and Challenges of Molecular Catalysts. *Chem. Soc. Rev.* **2019**, *48*, 2216−2264. (g) Kondo, M.; Tatewaki, H.; Masaoka, S. Design of Molecular Water Oxidation Catalysts with Earth-Abundant Metal Ions. *Chem. Soc. Rev.* **2021**, *50*, 6790−6831. (h) Das, P. K.; Bhunia, S.; Chakraborty, P.; Chatterjee, S.; Rana, A.; Peramaiah, K.; Alsabban, M. M.; Dutta, I.; Dey, A.; Huang, K. W. Electrocatalytic Water Oxidation by a Phosphorus-Nitrogen O = PN3-Pincer Cobalt Complex. *Inorg. Chem.* **2021**, *60*, 614−623. (i) Neuman, N. I.; Albold, U.; Ferretti, E.; Chandra, S.; Steinhauer, S.; Rossner, P.; Meyer, F.; Doctorovich, F.; Vaillard, S. E.; Sarkar, B. Cobalt Corroles as Electrocatalysts for Water Oxidation: Strong Effect of Substituents on Catalytic Activity. *Inorg. Chem.* **2020**, *59*, 16622−16634. (j) Garrido-Barros, P.; Moonshiram, D.; Gil-Sepulcre, M.; Pelosin, P.; Gimbert-Surinach, C.; Benet-Buchholz, J.; Llobet, A. Redox Metal-Ligand Cooperativity Enables Robust and Efficient Water Oxidation Catalysis at Neutral pH with Macrocyclic Copper Complexes. *J. Am. Chem. Soc.* **2020**, *142*, 17434−17446. (k) Liu, Y. J.; Han, Y. Z.; Zhang, Z. Y.; Zhang, W.; Lai, W. Z.; Wang, Y.; Cao, R. Low Overpotential Water Oxidation at Neutral pH Catalyzed by a Copper(II) Porphyrin. *Chem. Sci.* **2019**, *10*, 2613−2622. (l) Chakraborty, B.; Gan-Or, G.; Raula, M.; Gadot, E.; Weinstock, I. A. Design of an Inherently-stable Water Oxidation Catalyst. *Nat. Commun.* **2018**, *9*. DOI: 10.1038/s41467-018-07281-z (m) Folkman, S. J.; Soriano-Lopez, J.; Galan-Mascaros, J. R.; Finke, R. G. Electrochemically Driven Water-Oxidation Catalysis Beginning with Six Exemplary Cobalt Polyoxometalates: Is It Molecular, Homogeneous Catalysis or Electrode-Bound, Heterogeneous CoOx, Catalysis? *J. Am. Chem. Soc.* **2018**, *140*, 12040−12055. (n) Rudshteyn, B.; Fisher, K. J.; Lant, H. M. C.; Yang, K. R.; Mercado, B. Q.; Brudvig, G. W.; Crabtree, R. H.; Batista, V. S. Water-Nucleophilic Attack Mechanism for the $Cu^{II}(pyalk)_2$ Water-Oxidation Catalyst. *ACS Catal.* **2018**, *8*, 7952−7960. (o) Li, J.; Guttinger, R.; More, R.; Song, F.; Wan, W.; Patzke, G. R. Frontiers of Water Oxidation: the Quest for True Catalysts. *Chem. Soc. Rev.* **2017**, *46*, 6124−6147. (p) Li, N.; Liu, J.; Dong, B. X.; Lan, Y. Q. Polyoxometalate-Based Compounds for Photo- and Electrocatalytic Applications. *Angew. Chem., Int. Ed.* **2020**, *59*, 20779−20793. (q) Singh, C.; Mukhopadhyay, S.; Das, S. K. Polyoxometalate-Supported Bis(2,2'-bipyridine)mono(aqua)nickel-(II) Coordination Complex: an Efficient Electrocatalyst for Water Oxidation. *Inorg. Chem.* **2018**, *57*, 6479−6490. (r) Sullivan, K. P.;

Wieliczko, M.; Kim, M.; Yin, Q. S.; Collins-Wildman, D. L.; Mehta, A. K.; Bacsa, J.; Lu, X. L.; Geletii, Y. V.; Hill, C. L. Speciation and Dynamics in the $Co_4V_2W_{18}O_{68}^{(10-)}$/Co(II)(aq)/CoOx Catalytic Water Oxidation System. *ACS Catal.* **2018**, *8*, 11952−11959. (s) Sullivan, K. P.; Yin, Q. S.; Collins-Wildman, D. L.; Tao, M. L.; Geletii, Y. V.; Musaev, D. G.; Lian, T. Q.; Hill, C. L. Multi-Tasking POM Systems. *Front. Chem.* **2018**, *6*. DOI: 10.3389/fchem.2018.00365 (t) Yu, L.; Lin, J. Q.; Zheng, M.; Chen, M. D.; Ding, Y. Homogeneous Electrocatalytic Water Oxidation at Neutral pH by a Robust Trinuclear Copper(II)-substituted Polyoxometalate. *Chem. Commun.* **2018**, *54*, 354−357.

(3) (a) Blakemore, J. D.; Crabtree, R. H.; Brudvig, G. W. Molecular Catalysts for Water Oxidation. *Chem. Rev.* **2015**, *115*, 12974−13005. (b) Kärkäs, M. D.; Åkermark, B. Water Oxidation Using Earth-abundant Transition Metal Catalysts: Opportunities and Challenges. *Dalton Trans* **2016**, *45*, 14421−14461. (c) Mohamed, E. A.; Zahran, Z. N.; Naruta, Y. Covalent Bonds Immobilization of Cofacial Mn Porphyrin Dimers on an ITO Electrode for Efficient Water Oxidation in Aqueous Solutions. *J. Catal.* **2017**, *352*, 293−299. (d) Li, Y. X.; Yao, R. Q.; Chen, Y.; Xu, B. R.; Chen, C. H.; Zhang, C. X. Mimicking the Catalytic Center for the Water-Splitting Reaction in Photosystem II. *Catalysts* **2020**, 10. (e) Lee, H. B.; Marchiori, D. A.; Chatterjee, R.; Oyala, P. H.; Yano, J.; Britt, R. D.; Agapie, T. S = 3 Ground State for a Tetranuclear (Mn_4O_4)-O-IV Complex Mimicking the S-3 State of the Oxygen-Evolving Complex. *J. Am. Chem. Soc.* **2020**, *142*, 3753−3761. (f) Lee, H. B.; Shiau, A. A.; Marchiori, D. A.; Oyala, P. H.; Yoo, B. K.; Kaiser, J. T.; Rees, D. C.; Britt, R. D.; Agapie, T. $CaMn_3^{IV}O_4$ Cubane Models of the Oxygen-Evolving Complex: Spin Ground States S < 9/2 and the Effect of Oxo Protonation. *Angew. Chem., Int. Ed.* **2021**, *60*, 17671−17679. (g) Gluz, N.; Christou, G.; Maayan, G. The Role of the -OH Groups within Mn-12 Clusters in Electrocatalytic Water Oxidation. *Chem. Eur. J.* **2021**, *27*, 6034−6043. (h) Smith, P. F.; Deibert, B. J.; Kaushik, S.; Gardner, G.; Hwang, S.; Wang, H.; Al-Sharab, J. F.; Garfunkel, E.; Fabris, L.; Li, J.; Dismukes, G. C. Coordination Geometry and Oxidation State Requirements of Corner-Sharing MnO_6 Octahedra for Water Oxidation Catalysis: An Investigation of Manganite (γ-MnOOH). *ACS Catal.* **2016**, *6*, 2089−2099. (i) Ghosh, T.; Maayan, G. Efficient Homogeneous Electrocatalytic Water Oxidation by a Manganese Cluster with Overpotential of Only 74 mV. *Angew. Chem., Int. Ed.* **2019**, *58*, 2785−2790.

(4) (a) Ma, L.; Wang, Q.; Man, W.-L.; Kwong, H.-K.; Ko, C.-C.; Lau, T.-C. Cerium(IV)-Driven Water Oxidation Catalyzed by a Manganese(V)-Nitrido Complex. *Angew. Chem., Int. Ed.* **2015**, *54*, 5246−5249. (b) Luna, M. A.; Moyano, F.; Sereno, L.; D'Eramo, F. Spectroscopic and Electrochemical Studies of High-valent Water Soluble Manganese Porphyrine. Electrocatalytic Water Oxidation. *Electrochim. Acta* **2014**, *135*, 301−310. (c) Mousazade, Y.; Najafpour, M. M.; Bagheri, R.; Jaglicic, Z.; Singh, J. P.; Chae, K. H.; Song, Z. L.; Rodionova, M. V.; Voloshin, R. A.; Shen, J. R.; Ramakrishna, S.; Allakhverdiev, S. I. A Manganese(II) Phthalocyanine Under Water-oxidation Reaction: New Findings. *Dalton Trans* **2019**, *48*, 12147−12158. (d) Guan, J. Q.; Duan, Z. Y.; Zhang, F. X.; Kelly, S. D.; Si, R.; Dupuis, M.; Huang, Q. G.; Chen, J. Q.; Tang, C. H.; Li, C. Water Oxidation on a Mononuclear Manganese Heterogeneous Catalyst. *Nat. Catal.* **2018**, *1*, 870−877. (e) Li, Y.-Y.; Ye, K.; Siegbahn, P. E. M.; Liao, R.-Z. Mechanism of Water Oxidation Catalyzed by a Mononuclear Manganese Complex. *ChemSusChem* **2017**, *10*, 903−911.

(5) (a) Shimazaki, Y.; Nagano, T.; Takesue, H.; Ye, B.; Tani, F.; Naruta, Y. Characterization of a Dinuclear Mn^V=O Complex and Its Efficient Evolution of O_2 in the Presence of Water. *Angew. Chem., Int. Ed.* **2004**, *43*, 98−100. (b) Li, X.; Zhang, X.-P.; Guo, M.; Lv, B.; Guo, K.; Jin, X.; Zhang, W.; Lee, Y.-M.; Fukuzumi, S.; Nam, W.; Cao, R. Identifying Intermediates in Electrocatalytic Water Oxidation with a Manganese Corrole Complex. *J. Am. Chem. Soc.* **2021**, *143*, 14613−14621. (c) Gao, Y.; Åkermark, T.; Liu, J.; Sun, L.; Åkermark, B. Nucleophilic Attack of Hydroxide on a Mn^V Oxo Complex: A Model of the O-O Bond Formation in the Oxygen Evolving Complex of Photosystem II. *J. Am. Chem. Soc.* **2009**, *131*, 8726−8727. (d) Kim, S. H.; Park, H.; Seo, M. S.; Kubo, M.; Ogura, T.; Klajn, J.; Gryko, D. T.; Valentine, J. S.; Nam, W. Reversible O-O Bond Cleavage and Formation between Mn(IV)-Peroxo and Mn(V)-Oxo Corroles. *J. Am. Chem. Soc.* **2010**, *132*, 14030−14032. (e) Guo, M.; Lee, Y.-M.; Gupta, R.; Seo, M. S.; Ohta, T.; Wang, H.-H.; Liu, H.-Y.; Dhuri, S. N.; Sarangi, R.; Fukuzumi, S.; Nam, W. Dioxygen Activation and O−O Bond Formation Reactions by Manganese Corroles. *J. Am. Chem. Soc.* **2017**, *139*, 15858−15867.

(6) (a) Hu, K.; Sampaio, R. N.; Marquard, S. L.; Brennaman, M. K.; Tamaki, Y.; Meyer, T. J.; Meyer, G. J. A High-Valent Metal-Oxo Species Produced by Photoinduced One-Electron, Two-Proton Transfer Reactivity. *Inorg. Chem.* **2018**, *57*, 486−494. (b) Fisher, K. J.; Materna, K. L.; Mercado, B. Q.; Crabtree, R. H.; Brudvig, G. W. Electrocatalytic Water Oxidation by a Copper(II) Complex of an Oxidation-Resistant Ligand. *ACS Catal.* **2017**, *7*, 3384−3387.

(7) Jin, N.; Ibrahim, M.; Spiro, T. G.; Groves, J. T. Trans-dioxo Manganese(V) Porphyrins. *J. Am. Chem. Soc.* **2007**, *129*, 12416−12417.

(8) (a) Lahaye, D.; Groves, J. T. Modeling the Haloperoxidases: Reversible Oxygen Atom Transfer Between Bromide Ion and an Oxo-Mn(V) Porphyrin. *J. Inorg. Biochem.* **2007**, *101*, 1786−1797. (b) Umile, T. P.; Wang, D.; Groves, J. T. Dissection of the Mechanism of Manganese Porphyrin-Catalyzed Chlorine Dioxide Generation. *Inorg. Chem.* **2011**, *50*, 10353−10362.

(9) Jin, N.; Lahaye, D. E.; Groves, J. T. A "Push-Pull" Mechanism for Heterolytic O-O Bond Cleavage in Hydroperoxo Manganese Porphyrins. *Inorg. Chem.* **2010**, *49*, 11516−11524.

(10) Wang, D.; Groves, J. T. Efficient Water Oxidation Catalyzed by Homogeneous Cationic Cobalt Porphyrins: Critical Roles for the Buffer Base. *Proc. Natl. Acad. Sci. U.S.A.* **2013**, *110*, 15579−15584.

(11) For a single-site catalyst, the catalytic current i_{cat} is linearly dependent on the catalyst concentration C_{cat} according to the electrochemical equation $i_{cat} = nFAC_{cat}(Dk_{obs}C_{sub})^{1/2}$.

(12) Chen, Z.; Concepcion, J. J.; Hu, X.; Yang, W.; Hoertz, P. G.; Meyer, T. J. Concerted O Atom-proton Transfer in the O-O Bond Forming Step in Water Oxidation. *Proc. Natl. Acad. Sci. U.S.A.* **2010**, *107*, 7225−7229.

(13) Bard, A. J.; Faulkner, L. R. Electrode Reactions with Coupled Homogeneous Chemical Reactions. In *Electrochemical methods: fundamentals and applications*; Harris, D., Ed.; John Wiley & Sons Inc.: Hoboken, NJ, 2001; pp 471−534.

(14) Matheu, R.; Neudeck, S.; Meyer, F.; Sala, X.; Llobet, A. Foot of the Wave Analysis for Mechanistic Elucidation and Benchmarking Applications in Molecular Water Oxidation Catalysis. *ChemSusChem* **2016**, *9*, 3361−3369.

(15) (a) Young, K. J.; Takase, M. K.; Brudvig, G. W. An Anionic N-Donor Ligand Promotes Manganese-Catalyzed Water Oxidation. *Inorg. Chem.* **2013**, *52*, 7615−7622. (b) Limburg, J.; Vrettos, J. S.; Chen, H.; de Paula, J. C.; Crabtree, R. H.; Brudvig, G. W. Characterization of the O_2-Evolving Reaction Catalyzed by $[(terpy)(H_2O)Mn^{III}(O)_2Mn^{IV}(OH_2)(terpy)](NO_3)_3$ (terpy = 2,2':6,2"-Terpyridine). *J. Am. Chem. Soc.* **2001**, *123*, 423−430. (c) Brimblecombe, R.; Kolling, D. R. J.; Bond, A. M.; Dismukes, G. C.; Swiegers, G. F.; Spiccia, L. Sustained Water Oxidation by $[Mn_4O_4]^{7+}$ Core Complexes Inspired by Oxygenic Photosynthesis. *Inorg. Chem.* **2009**, *48*, 7269−7279. (d) Kurz, P.; Berggren, G.; Anderlund, M. F.; Styring, S. Oxygen Evolving Reactions Catalysed by Synthetic Manganese Complexes: A Systematic Screening. *Dalton Trans* **2007**, 4258−4261.

(16) den Boer, D.; Siberie, Q.; Siegler, M. A.; Ferber, T. H.; Moritz, D. C.; Hofmann, J. P.; Hetterscheid, D. G. H. On the Homogeneity of a Cobalt-Based Water Oxidation Catalyst. *ACS Catal.* **2022**, *12*, 4597−4607.

(17) Vanysek, P. Electrochemical Series. *CRC Handbook of Chemistry and Physics*; Taylor & Francis, 2010.

(18) Swain, C. G.; Scott, C. B. Quantitative Correlation of Relative Rates. Comparison of Hydroxide Ion with Other Nucleophilic Reagents toward Alkyl Halides, Esters, Epoxides and Acyl Halides. *J. Am. Chem. Soc.* **1953**, *75*, 141−147.

https://doi.org/10.1021/acs.inorgchem.2c02284
Inorg. Chem. 2022, 61, 13667−13672

(19) Jin, N.; Bourassa, J. L.; Tizio, S. C.; Groves, J. T. Rapid, Reversible Oxygen Atom Transfer between an Oxomanganese(V) Porphyrin and Bromide: A Haloperoxidase Mimic with Enzymatic Rates. *Angew. Chem., Int. Ed.* **2000**, *39*, 3849−3851.
(20) (a) Pokhrel, R.; Service, R. J.; Debus, R. J.; Brudvig, G. W. Mutation of Lysine 317 in the D2 Subunit of Photosystem II Alters Chloride Binding and Proton Transport. *Biochemistry* **2013**, *52*, 4758−4773. (b) Mandal, M.; Askerka, M.; Banerjee, G.; Amin, M.; Brudvig, G. W.; Batista, V. S.; Gunner, M. R. Characterization of Ammonia Binding to the Second Coordination Shell of the Oxygen-evolving Complex of Photosystem II. *Dalton Trans* **2017**, *46*, 16089−16095. (c) Brahmachari, U.; Gonthier, J. F.; Sherrill, C. D.; Barry, B. A. Chloride Maintains a Protonated Internal Water Network in the Photosynthetic Oxygen Evolving Complex. *J. Phys. Chem. B* **2017**, *121*, 10327−10337.
(21) (a) Kawakami, K.; Umena, Y.; Kamiya, N.; Shen, J.-R. Location of Chloride and Its Possible Functions in Oxygen-evolving Photosystem II Revealed by X-ray Crystallography. *Proc. Natl. Acad. Sci. U.S.A.* **2009**, *106*, 8567−8572. (b) Umena, Y.; Kawakami, K.; Shen, J.-R.; Kamiya, N. Crystal Structure of Oxygen-evolving Photosystem II at a Resolution of 1.9 A. *Nature* **2011**, *473*, 55−60. (c) Wang, J. M.; Perez-Cruet, J. M.; Huang, H. L.; Reiss, K.; Gisriel, C. J.; Banerjee, G.; Kaur, D.; Ghosh, I.; Dziarski, A.; Gunner, M. R.; Batista, V. S.; Brudvig, G. W. Identification of a Na^{+}-Binding Site near the Oxygen-Evolving Complex of Spinach Photosystem II. *Biochemistry* **2020**, *59*, 2823−2831.
(22) Wang, L.; Zhang, C.; Zhao, J. Location and Function of the High-affinity Chloride in the Oxygen-evolving Complex − Implications from Comparing Studies on Cl/Br/I-substituted Photosystem II Prepared Using Two Different Methods. *J. Photoch Photobio B* **2014**, *138*, 249−255.

https://doi.org/10.1021/acs.inorgchem.2c02284
Inorg. Chem. 2022, 61, 13667−13672